# Phase Transitions and Polymorphism of Cocoa Butter

**C. Loisel[a,b], G. Keller[a], G. Lecq[b], C. Bourgaux[c], and M. Ollivon[a,*]**

[a]Laboratoire de Physico-Chimie des Systèmes Polyphasés, Université Paris-Sud, 92296 Châtenay-Malabry, France, [b]Centre Jean Thèves, groupe DANONE, Branche Biscuits, 91207 Athis-Mons Cedex, France, and [c]Laboratoire pour l'Utilisation du Rayonnement Electromagnétique, Université Paris-Sud, 91405 Orsay, France

**ABSTRACT:** The polymorphism and phase transitions of cocoa butter (CB) have been reexamined separately by differential scanning calorimetry (DSC) and X-ray diffraction as a function of temperature (XRDT) at scanning rates between 0.1 to 5°C/min and 0.1 to 2°C/min, respectively. A new instrument, which allowed simultaneous DSC and XRDT recordings from the same sample by taking advantage of the high-energy flux of a synchrotron, was employed for characterization of the intermediate phase transitions. These techniques allowed us to confirm the existence of the six polymorphic forms of CB (called I to VI) by *in situ* characterization of their formation in the DSC + XRDT sample holder. A detailed study of Form I structure led us to propose a liquid-crystal organization in which some of the chains displayed sharp long-spacing lines ($d_{001}$ = 52.6 ± 0.5 Å) and a β′ organization (4.19 and 3.77 Å), while the others remained unordered with broad scattering (maxima at about 112 and 36.5 Å). The organization of this liquid crystalline phase is compared to that of fat and oil liquids. This liquid crystalline phase progressively transformed on heating into a more stable phase (Form II, α type, $d_{001}$ = 48.5 ± 0.5 Å and short-spacing at 4.22 Å). Form III was only observed in a sharp temperature domain through its specific short-spacings. The existence of the six species has been essentially related to the crystallization of monounsaturated triacylglycerols (TAG), while trisaturated species were found partly solid-soluble in these six polymorphic forms. An insoluble fraction crystallized independently of the polymorphism of the monounsaturated TAG in a separate phase with long-spacings that were either of the α (49.6 ± 0.5 Å) or β (44.2 ± 0.5 Å) form. In mixture with Form V, this fraction melts and solubilizes in the liquid phase at 37.5°C. Isolation of these high-melting crystals shows a melting point of about 50°C. High-performance liquid chromatography analysis of this fraction confirmed an increase from 3.0 to 11.3% of saturated TAG and their association with part of the 1,3-stearoyl-2-oleoylglycerol preferentially to 1-palmitoyl-2-oleoyl-3-stearoylglycerol and (1,3-palmitoyl-2-oleoylglycerol).
*JAOCS 75*, 425–439 (1998).

**KEY WORDS**: Chocolate crystallization, cocoa butter, DSC, liquid crystals, palm oil, phase transitions, polymorphism, triacylglycerols, X-ray diffraction.

Natural fats are mainly composed of triacylglycerols (TAG) in which some minor compounds are solubilized. Their TAG composition determines their physical, in particular their thermal, properties. While most, but especially animal, fats are composed of complex mixtures of numerous TAG, some vegetable fats, such as cocoa butter (CB), have a simpler composition. This fat is composed of a mixture of three classes of TAG (saturated, monounsaturated, and polyunsaturated TAG), the monounsaturated being by far the major component because they represent more than 80% of the total. Moreover, only three TAG [1,3-palmitoyl-2-oleoylglycerol (POP), 1-palmitoyl-2-oleoyl-3-stearoylglycerol (POSt), and 1,3-stearoyl-2-oleoylglycerol (StOSt)] account for more than 95% of this fraction. Polyunsaturated and trisaturated TAG correspond to about 13 and 3%, respectively, of the TAG content. This specificity gives CB a thermal and structural behavior similar to that of a pure compound. This behavior is nevertheless complex because all major TAG in its composition, like most lipids, themselves show complex polymorphism (e.g., six different polymorphic varieties have been observed for POP) (1).

Fat polymorphism and TAG crystallization have been studied for more than a century. Polymorphism results from the different possibilities of lateral packing of the fatty acid chains and of the longitudinal stacking of molecules in lamellae (1–6). These two levels of organization are easily identifiable from the short- and long-spacings observed by X-ray diffraction (XRD) at wide and small angles, respectively. The three main organizations frequently observed for the lateral packing of TAG, called α, β′ and β, in the order of their increasing stability, have been related to different subcells that have been described in detail (2–6).

The lipid long-spacings correspond to the repeat distance in the direction perpendicular to the lamellae. For TAG, long-spacings are commonly double or triple chainlengths (2L or 3L). A fourth crystalline structure, often called sub-α, although it contains a β′ subcell and would be less stable than the α form, is also reported in the literature (7). Moreover, the existence of a liquid state of TAG, which is also organized as a liquid crystalline phase, is still under debate (3,8,9).

The polymorphism of CB, which is a vegetable fat mainly used by chocolate manufacturers, has often been discussed in the literature because it is related to the organoleptic and

*To whom correspondence should be addressed at Laboratoire de Physico-Chimie des Systèmes Polyphasés, CNRS URA 1218, Université Paris-Sud, 92296 Châtenay-Malabry, France. E-mail: ollivon@psisun.u-psud.fr.

**TABLE 1**
**Long- and Short-Spacings (Å) of the Different Polymorphic Forms of Cocoa Butter (literature values)[a]**

| Reference | I (2L)[b] β′-sub(α) | II (2L)[b] α | III (2L)[b] $\beta'_2$ | IV (2L)[b] $\beta'_1$ | V (3L)[b] $\beta_2$ | VI (3L)[b] $\beta_1$ |
|---|---|---|---|---|---|---|
| 10 | 4.19 (vs) | 49 (vs)[c] | 49 (vs)[c] | 45 (vs)[c] | 63.1 (m)[c] | 63.1 (vs)[c] |
| | 3.70 (s) | 16.3 (s)[c] | 4.25 (vs) | 14.87 (s)[c] | 32.2 (vs)[c] | 32 (?)[c] |
| | | 4.24 (vs) | 3.86 (s) | 4.35 (vs) | 12.8 (s)[c] | 12.76 (s)[c] |
| | | | | 4.15 (vs) | 4.58 (vs) | 4.59 (vs) |
| | | | | | 3.98 (vs) | 3.70 (s) |
| | | | | | 3.67 (w) | |
| 15 | 54 (s)[c] | 51 (vs)[c] | 51 (vs)[c] | 49 (vs)[c] | 66 (s)[c] | 63 (s)[c] |
| | 4.17 (s) | 4.20 (vs) | 4.20 (vs) | 14.8 (w)[c] | 33 (s)[c] | 31 (s)[c] |
| | 3.87 (m) | | 3.87 (w) | 4.32 (s) | 12.8 (m)[c] | 12.7 (mw)[c] |
| | | | | 4.13 (s) | 4.58 (vs) | 4.53 (vs) |
| | | | | | 3.98 (ms) | 3.84 (m) |
| | | | | | 3.65 (ms) | 3.67 (s) |
| 16 | | | | 45[c] | 64[c] | 63.8[c] |
| | | | | 4.35 | 4.58 | 4.59 |
| | | | | 4.15 | 3.98 | 3.7 |

[a]vs = very strong, s = strong, ms = medium strong, mw = medium weak, w = weak.
[b]2L, 3L = number of hydrocarbon chains in the crystalline structure.
[c]Long-spacings.

physical characteristics of the final products (snap, molding contraction, gloss and blooming during storage). It often has been compared to that of POP, POSt and StOSt (about 17, 37, and 27% of the fat, respectively) and that of their mixtures (1,6,10–13). CB polymorphism is commonly described in the literature in terms of six different polymorphic forms, noted from I to VI in increasing order of melting points, according to the nomenclature of Wille and Lutton (10,14–20; Tables 1 and 2). Although these six forms have been confirmed by other authors (15,17–20), the existence of some of them is debated. According to some authors (10,19,21,22), Form III corresponds to a mixture of Forms II and IV and is not a separate crystalline variety. In the same way, Form I could be a phase mixture (10), and Form VI may result from phase separation within a solid solution (19,21,23). More recently, van Malssen (24) criticized the designation of solid states of complex mixtures, crystallized as polycrystalline aggregates, as different polymorphs when the chemical compositions of the different crystallites are not identical. According to him, several polymorphs of CB and at least the phases sub-α, α, and β′ probably correspond to nonhomogeneous crystalline states.

Davis and Dimick (25,26) postulated and verified by the analysis of seed crystals that some minor components, such as glycolipids (11.1%), phospholipids (6.6%) and saturated TAG (67.7%), promote the crystallization of CB. Moreover, it has been found that CB crystallization is related to its composition (27,28). Cebula *et al.* (29) observed that trisaturated TAG did not hinder the formation of the appropriate amounts of symmetrical TAG seeds during chocolate tempering.

Recently, access to high-flux sources (synchrotron) has permitted study of the thermal behavior of pure TAG by XRD as a function of temperature (XRDT) (30–33). This technique allows quantitative monitoring of the evolution of both long- and short-spacings as a function of temperature, for instance during phase transitions that occur on heating of unstable species of pure compounds. More recently, the polymorphism and phase transitions displayed by complex TAG mixtures also have been characterized by XRDT and compared to differential scanning calorimetry (DSC) recordings (34). Lavigne (35) used these techniques to study the thermal behavior of anhydrous milk fat and its fractions. Chemical TAG analysis of each fraction allowed the complex thermal profiles recorded by DSC to be decomposed into elementary phase transitions and to identify the TAG involved in each of them. A model of the molecular organization of the β′ phase of complex fat mixtures was proposed (35). This demonstrates that the combination of these two techniques of thermal analysis is especially suitable for the characterization of co-

**TABLE 2**
**Melting Point (°C) of the Different Polymorphic Forms of Cocoa Butter (literature values)**

| References | | | | | | |
|---|---|---|---|---|---|---|
| 14 | 10 | 15 | 17 | 18 | 19 | 20 |
| 18 (γ) | 17.3 (I) | | 14.9–16.1 (I) | 13 (VI) | 16–18 (γ) | 13.1 (I) |
| 23.5 (α) | 23.3 (II) | | 17–23.2 (II) | 20 (V) | 20.7–24.2 (α) | 17.7 (II) |
| | 25.5 (III) | 20.7 (III) | 22.8–27.1 (III) | 23 (IV) | | 22.4 (III) |
| 28 (β″) | 27.5 (IV) | 25.6 (IV) | 25.1–27.4 (IV) | 25 (III) | 26–28 (β′) | 26.4 (IV) |
| 33 (β′) | 33.87 (V) | 30.8 (V) | 31.3–33.2 (V) | 30 (II) | 33.7–34.9 (β) | 30.7 (V) |
| 34 (β) | 36.3 (VI) | 32.3 (VI) | 33.8–36 (VI) | 33.5 (I) | | 33.8 (VI) |

existing organizations that result from the phase separations frequently occurring in complex fat mixtures.

The aim of this paper is to extend this approach to a fat that is considered to behave as a pure compound, in studying, by combined and simultaneous DSC and XRDT, the complex phase transitions that occur during CB crystallization and melting. The high energy of the synchrotron source allows possible phase separations to be detected and the competition between the different polymorphic species to be followed quantitatively, even at fast scanning rates, in the short-spacing domain at large angles as well as in the long-spacing domain at very small angles.

## MATERIALS AND METHODS

*Samples.* The CB used was a standard factory product that originated from the Ivory Coast. Its composition, determined by gas chromatography (norm ISO 5508/5509) and high-performance liquid chromatography (HPLC) (IUPAC 2.324) for TAG analysis and by atomic absorption (IUPAC 2-423; see Ref. 6, Chapter 14, for these methods) for phospholipid content, was as follows: TAG 97%; diacylglycerols 1.1%; monoacylglycerols 0.2%; free fatty acids 1.3%; phosphatides 0.15%; others 0.25%. The TAG composition is reported in Table 3. Pure palm oil and its fractions (low- and high-melting fractions) were donated by Sanofi-Soprorga (Saint Denis, France). Tristearin (StStSt) and POP were synthesized in the laboratory (36), POP was further purified by HPLC (35) (the purity of both was about 99.9%). Triolein (99%) was from Sigma (l'Isle d'Abeau, France).

*CB fractionation.* CB fractions were obtained after 3 wk of storage at 30.0 ± 0.5°C, in tubes capped under argon gas, after initial melting at 80°C over about 10 min. At the end of this incubation time, the crystals [high-melting fraction (HMF)] and the liquid [low-melting fraction (LMF)] were isolated by centrifugation at 30 ± 1°C and 64,000 × *g* (Sigma; model 3K30) in a preheated rotor. The separated HMF was isolated by aspirating most of the liquid fraction with a pipette and then eliminating the residual liquid with blotting paper. This separation took less than 2 min at room temperature (21 ± 1°C). Samples were stored at 4°C before thermal and XRD analysis. TAG compositions of these fractions were determined as above.

*XRD.* XRD was performed with either a classical installation (Enraf-Nonius, Cu, 40 kV, 20 mA; Gagny, France) and a goniometer (Seifert; Alexandre Labo, Toulouse, France) or with the high-energy synchrotron beam at L.U.R.E. (Laboratoire pour l'Utilisation du Rayonnement Electromagnétique, Orsay, France) by using the D24 station (about $5 \cdot 10^9$ photons/s/mm$^2$) operated at $\lambda = 1.488$ Å. Both installations were equipped with Peltier temperature-controlled sample holders, which recently have been described (34).

Briefly, single-stage Peltier modules (Melcor, AMS Electronic, Les Ulis, France) were used to cool these devices (below −20°C in the absence of heating), while heating was monitored by a temperature controller (Eurotherm 902P, Dardilly, France) with a type E thermocouple as sensor. When associated with a cryostat (Lauda, RCS6; Königshofen, Germany), these sample holders allow heating or cooling of the sample at rates ranging from 0.1 to 10°C/min. Gas-filled linear detectors (1024 channels, either filled with Ar or a Xe–$CO_2$ mixture) were used for data collection. Standardization was carried out with the form β of pure StStSt, which is characterized by a long-spacing of 44.98 Å at room temperature (6).

All XRD patterns were recorded by transmission through glass capillaries (GLAS, Berlin, Germany). Samples were prepared by filling these glass capillaries with about 20–30 µL of melted fats at temperatures about 20°C above their final melting points and centrifuging them immediately before fat solidification could take place. Quenching of these capillaries with the melted samples was first accomplished either by placing them rapidly in contact with a metal block cooled to −30°C and then transferring them to the precooled sample holder (−10°C), or by directly introducing them into the latter. A more convenient technique was developed to prevent breakage of the capillary and uncontrolled solid–solid heat transfer. Very fast quenching was attained by plunging capillaries into a vessel with ethanol maintained at −30 or −70°C.

Form V of CB was prepared by rapid crystallization at 21 ± 1°C in a glass capillary and storage for 1 wk at this temperature. Depending on heating or cooling rates, the time of exposure corresponding to one recording of a diffraction pattern was between 60 s (2°C/min) and 300 s (0.1°C/min). Two experimental setups were employed, and most of the XRDT experiments were recorded twice, the first at short sample-detector distance ($d$ = 290 mm) to determine events at both short- and long-spacings simultaneously, and then at long dis-

**TABLE 3**
**Concentration of TAG in Initial and Fractionated Cocoa Butter (wt%)[a]**

| TAG | Low-melting fraction | Initial cocoa butter | High-melting fraction |
|---|---|---|---|
| OLO | 0.4 | 0.4 | 0.4 |
| PLO | 0.4 | 0.5 | 0.3 |
| PLP | 1.7 | 1.6 | 1.1 |
| OOO | 0.2 | 0.4 | 0.2 |
| POO | 2.8 | 2.8 | 2.2 |
| PLSt | 1.5 | 1.4 | 1.1 |
| StOO | 3.3 | 3.4 | 3.1 |
| StLSt | 3.2 | 3.0 | 2.6 |
| POP | 17.3 | 17.0 | 14.8 |
| POSt | 37.3 | 36.6 | 34.1 |
| StOSt | 27.3 | 27.3 | 27.4 |
| StOAr | 1.8 | 1.9 | 1.4 |
| PPSt | 1.3 | 1.4 | 3.4 |
| PStSt | 0.6 | 1.1 | 4.8 |
| StStSt | 0.4 | 0.5 | 3.1 |
| Saturated TAG | 2.3 | 3.0 | 11.3 |
| Monounsaturated TAG | 83.7 | 82.8 | 77.7 |
| Polyunsaturated TAG | 13.5 | 13.5 | 11.0 |
| Total | 99.5 | 99.3 | 100.0 |

[a]Abbreviations: Ar: arachidic acid, (C 20:0); L: linoleic acid, (C 18:2); O: oleic acid, (C 18:1); P: palmitic acid, (C 16:0); St: stearic acid, (C 18:0). TAG, triacylglycerols.

tance ($d$ = 1450 mm) to obtain a better resolution of long-spacing lines at small angles (0–2°).

Because the intensities of the diffraction peaks varied as a function of temperature during XRDT recordings, they were normalized as follows. At temperature $T$, the intensity of a line $I_T$ was determined either by an X-ray analysis computer program (37) or by quadratic regression analysis of the data that corresponded to the peak maximum and its surroundings. The normalized intensities were calculated from that of maximum $I_{max}$ and minimum $I_{min}$ : $I_{T\%} = 100 \cdot (I_T - I_{min})/ (I_{max} - I_{min})$.

*DSC.* Thermal analyses were conducted on a Perkin-Elmer (St. Quentin en Yvelines, France) differential scanning calorimeter (DSC-7) in aluminum pans of 40 µL (pan, part #B014-3024 and cover, part #B014-3004). Calibration was made with lauric acid (purity >99.9%), so that temperature and enthalpies could be corrected for each heating rate, as previously described (38). Unstable species were studied by quenching melted CB (80°C) at –40°C (in less than 1 s) and subsequent heating at 0.1, 1, and 2°C/min. Intermediate species of fractionated and pure CB were studied by cooling the melted CB at –2°C/min and heating it at 5°C/min. The peak temperatures were taken at the maxima of the endotherms instead of the onsets because of peak overlapping. Therefore, the melting points observed for the different polymorphic varieties at these peak maxima were systematically higher than the values reported in the literature or measured at onset (39).

## RESULTS

*More stable forms. XRD.* XRDT of CB (Form V) was recorded every minute during heating at 1°C/min from 25 to 34°C and at 0.3°C/min from 34 to 41°C. The long- and short-spacings observed at 25°C with the short sample-detector distance (LS = 66 and 33 Å; SS = 4.58, 3.98, 3.89, 3.77, and 3.67 Å) confirmed, as expected, the crystallization of CB into a β-3L structure (Form V, Table 1). A weak line at about $q$ = 0.14 $Å^{-1}$, corresponding to a long-spacing of 44.4 Å, was also observed at 25°C and was confirmed on recordings obtained at long sample-detector distance (Fig. 1). The evolution of the intensity of this line as a function of temperature (between 25

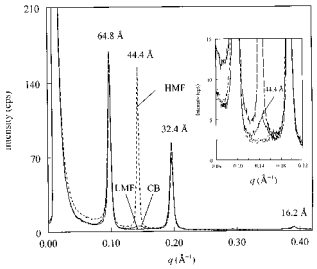


**FIG. 1.** Small-angle X-ray diffraction (XRD) recordings of Form V of cocoa butter (CB) (solid line) and of its high-(HMF) and low-melting (LMF) fractions. Insert shows Form V of CB on an enlarged y scale.

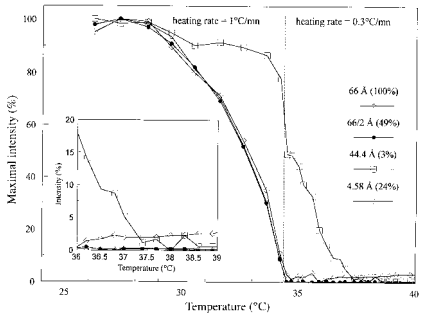


**FIG. 2.** Evolution of the intensities of the small-angle XRD spacings of Form V of CB between 25 and 40°C. For each spacing, a series of lines is observed, the intensities of which have been expressed as a percentage of the peak maximum. Absolute intensities observed for Form V of CB are shown in Figure 1. Relative intensities of the peaks are given on the graph within parentheses: 100% corresponds to the strongest peak. Insert: enlarged scale. See Figure 1 for abbreviations.

and 41°C) was compared to that of the β-3L (V) structure (Fig. 2) by using data recorded with the short sample-detector distance. Above 34.5°C, all lines (long- and short-spacings) that characterize Form V disappeared (they were progressively replaced by the bumps that correspond to scattering from the liquid organization), except the line at 44.4 Å, which finally vanished at 37.5°C. The observation at 25°C of a line at 44.4 Å was first interpreted as the presence, in β-3L (Form V), of a trace amount of the β′ form (Form IV) because the latter is characterized by a similar long-spacing at about 45 Å (Table 1). However, the melting point of this form, within the temperature interval 25–28°C (Table 2), is clearly incompatible with the persistence of the line observed by XRDT above 37°C and rules out this hypothesis, even taking into account the heating rate of 1°C/min, because melting of Form V ends at 34.5°C.

These results show that a lipid segregation occurs in CB on cooling and/or during storage. If the segregation occurs during cooling, it would be a rapid process because sample crystallization was observed in the capillary after a few seconds (see the Materials and Methods section). The fraction that crystallizes in addition to the usual β-3L form (V) exhibits a higher melting point than Form V and a long-spacing (44.4 Å) that corresponds to a 2L packing close to that of the β form of StStSt (about 45 Å, see above).

This behavior may be considered in the light of recent DSC observations made by Davis and Dimick (25,26) on CB crystallization. They found that crystallization at 26.5°C starts by the formation of seed crystals that are characterized by a high melting point (up to 72.4°C). Compared to the original CB, these crystals are enriched in glycolipids, phospholipids, and the saturated TAG [1,2-palmitoyl-3-stearoyl glycerol (PPSt), 1-palmitoyl-2,3-stearoyl glycerol (PStSt), and tristearoylglycerol (StStSt)]. We also observed the formation of a cloudy fraction in the liquid CB, initially isotropic, after a few hours' storage at 26.5°C. At the same time, it was necessary to increase the sample temperature to above 45°C to melt this fraction. Taking into account the similar conditions of crystal formation in all samples, we decided to further characterize this fraction by XRD, DSC, and chemical analysis.

*Chemical and XRD analysis of the fractions.* Partial crystallization of a CB sample was carried out by conditioning its melt at 30.0 ± 0.5°C for 3 wk. As above, a cloudy and dense fraction was separated from the liquid. Two fractions, HMF and LMF, were isolated at 30.0 ± 1.0°C and analyzed as described in the Materials and Methods section. Small-angle XRD analysis of these two fractions, reported in Figure 1, showed that the HMF long-spacings were characterized by a stronger intensity of the line at 44.4 Å than that of the initial CB. This diffraction line was not detected in the LMF. No significant difference was observed in the short-spacings between HMF, LMF, and initial CB.

The TAG compositions of these two fractions are reported in Table 3. The HMF showed a higher concentration of trisaturated TAG (11.3%) and a lower content in polyunsaturated TAG (11%) compared with the initial CB (3.0 and 13.5%, respectively) and its LMF (2.3 and 13.5%, respectively). TAG analysis shows that StStSt, PStSt, and PPSt concentrations were increased about 8, 7, and 2.5 times, respectively, in the HMF compared with LMF. On the other hand, a decrease of monounsaturated TAG was observed in HMF (77.7%) compared with LMF (83.7%), which was specific for POP (14.8/17.3) and for POSt (34.1/37.3), while StOSt was found to be constant in the two fractions (27.4/27.3). Fatty acid analysis confirmed these results and showed an increase of stearic acid from 36.4 to 41.6%, from LMF to HMF, while palmitic, oleic, and linoleic acids decreased from 25.5 to 24.6%, 33.1 to 29.3%, and 2.6 to 2.1%, respectively. So, XRD lines at 66 and 33 Å, observed in the HMF (Fig. 1), can be attributed to the crystallization of a β-3L form of monounsaturated TAG, while the line at 44.4 Å is related to that of the StStSt.

*Thermal analysis.* Thermal analysis was successively conducted at –2°C/min on cooling between 60 and –40°C and at +5°C/min in the same temperature range, with pure CB, HMF, and LMF samples. In the DSC recordings reported in Figure 3A, three peaks appeared during pure CB crystallization, at 19.2, 14.2, and 1.7°C. During the crystallization of

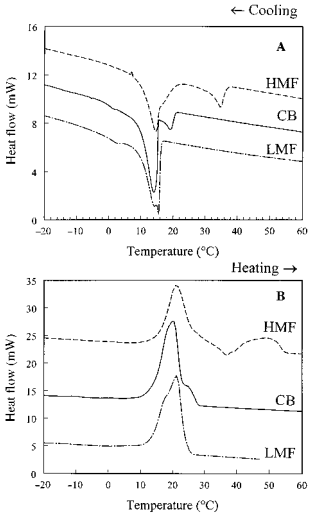


**FIG. 3.** Differential scanning calorimetry (DSC) recordings of crystallization (A, cooling rate = 2°C/min) and melting (B, heating rate = 5°C/min) of CB. See Figure 1 for other abbreviations.

HMF (Fig. 3A), the first peak at 19.2°C increased to 34.7°C, while it was absent from LMF (Fig. 3A). Furthermore, the peak at 1.7°C increased to 4°C for LMF and was absent from HMF. The single peak at 14.2°C for the pure CB gave a double peak at 15 and 17°C for HMF and at 15.2 and 16.3°C for LMF. Indeed, the large increase of the initial crystallization temperature on DSC recordings confirmed that phase separation occurred between a minor fraction with a high melting point and a major fraction composed of the other TAG. Similarly, the weak exothermic events observed at about 4°C, the enthalpy of which increased for LMF, are probably related to another phase separation that occurs between polyunsaturated and monounsaturated TAG.

The corresponding melting recordings (Fig. 3B) show that the increase of trisaturated TAG content in HMF led to the formation of an endotherm at about 50°C (Fig. 3B), while its decrease in LMF (Fig. 3B) led to the disappearance of the peak observed with pure CB at 24.9°C (Fig. 3B). The origin of this endotherm will be discussed below (see the Intermediate forms section). The exotherm at 37°C for HMF (Fig. 3B) shows that recrystallization occurred at this temperature, and melting of the species formed at this point spread up to about 50°C. The incorporation of 2% StStSt in pure CB confirmed that this polymorphic transition was related to trisaturated TAG crystallization (see below). On this occasion, a different analysis carried out with CB enriched with StStSt (data not presented here) showed that a decrease of the cooling rate from 5 to 0.5°C/min induced increases of the peak temperatures shown in Figure 3A (HMF curve ) from 24.0 to 28.9°C for the first exotherm and from 13 to 15.4°C for the second. These temperature shifts were comparable to those observed between HMF and CB curves (Fig. 3A). Whatever the cooling rate, the last endotherm observed on heating at 5°C/min (Fig. 3B, HMF curve for comparison) was found at a constant temperature (49.8 ± 0.1°C). However, a decrease of the cooling rate induced an increase of the exotherm temperature (observed on Fig. 3B, HMF) from 35.8 to 38.2°C. This indicates that trisaturated TAG probably crystallize into an unstable form (likely to be α) before transformation to their more stable form (β).

The formation of Form VI of CB, its thermal and structural properties, and its coexistence with variety V already have been addressed previously and therefore will not be reexamined in this study (16,34,40).

*Unstable forms. XRD.* Metastable forms were studied by quenching melted CB from 80 to −10°C at about 100°C/s. Small-angle XRD, recorded at −10°C, shows that the long-spacings of CB decomposed into two sharp lines that correspond to spacings of about 52.6 Å ($q$ = 0.12 Å$^{-1}$) and 26.3 Å ($q$ = 0.24 Å$^{-1}$) and two broad scattering peaks that are centered, respectively, at about $q$ = 0.17 Å$^{-1}$ (intense, 36.4 Å) and $q$ = 0.06 Å$^{-1}$ (weak, 112 Å) (Fig. 4A). Short-spacings observed together with long-spacings during a second experiment, performed at a shorter sample-detector distance but under the same conditions, are given in Figure 4B and show the existence of two spacings at 4.19 and 3.77 Å above a broad

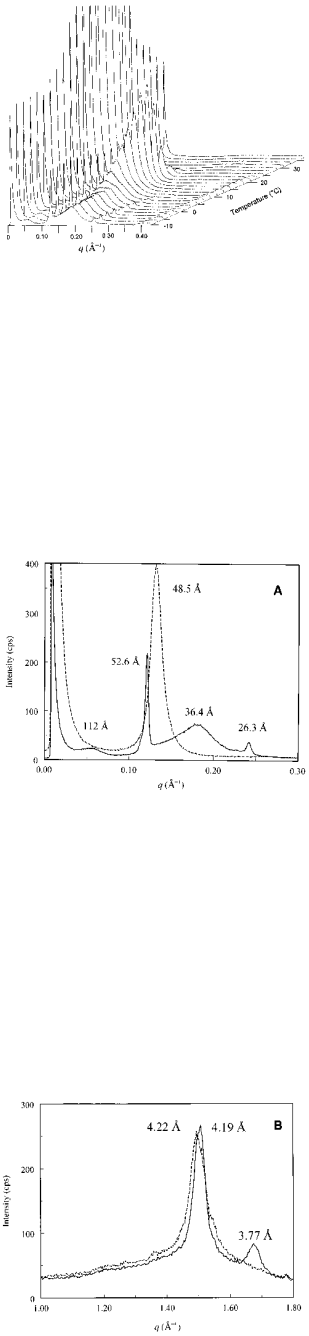


**FIG. 4.** Three-dimensional plot for the evolution of the long-spacings of CB as determined by small-angle XRD during heating of a sample that was obtained by liquid quenching at 100°C/s from −10 to 40°C at 1°C/min. Part A shows the long-spacings observed at −10°C, before, and at 20°C, after transition to the α form. Part B shows the corresponding short-spacings. ——, −10°C; ------, 20°C. See Figure 1 for abbreviations.

scattering peak at about $q$ = 1.4–1.5 Å$^{-1}$. Figure 4 also shows the evolution of the long-spacings recorded at 1°C/min between −10 and 40°C. We see that the sharp and broad peaks, the initial repeat distances of which are 52.6 and 36.4 Å, tend progressively to merge into a single large peak at 48.5 Å (the third order of which was also observed at 16.1 Å during the second experiment).

To determine the correspondence of the different lines, variations of their intensities between −10 and 40°C were plotted on the same graph (Fig. 5A and 5B). It appears that the line at 52.6 Å may be related to the line at 3.77 Å because they decrease simultaneously. The broad peak at 36.4 Å does not seem to correspond to the same polymorphic form, because its evolution is different from the evolution of the former lines, but this evolution is probably related to the increase of the line at 48.5 Å. The lower intensity of the line at 112 Å prevents precisely plotting its evolution, which apparently follows that of the three other lines. The disappearance of the long-spacings at 52.6 Å was accompanied by the appearance of a new line at 48.5 Å and by the evolution of the short-spacings at 4.19 and 3.77 Å toward a single line at 4.22 Å. However, this evolution was preceded by a shift of the 3.77 Å spacing toward about 3.85 Å. This observation may explain the 3.87 Å value reported by Chapman *et al.* (15) for Form I of CB (Table 1). Further heating above 20°C slowly shifts the spacing at 48.5 Å to give a weak line at 44.9 Å, which in turn completely disappears below 30°C (arrow in Fig. 5A).

Thermal analysis, recorded simultaneously with XRD from the same sample during heating, achieved through XRDT–DSC coupling, is reported in Figure 5C. The two recordings presented correspond to the two different sample-detector distances. Exotherms at 0°C result from melting of some ice crystals formed on the capillary tube during quenching of CB. Figures 5A and 5B show that the decreases of the lines corresponding to spacings at 52.6 and 3.77 Å are correlated with the increase of the line at 48.5 Å (also seen for third order, data not shown). However, no clear endotherm is associated with this transition, in contrast to what was observed beyond 15°C for further transitions. This would mean that this polymorphic transition is energetically low and/or extends over a large domain of temperature. Its irreversible character can be deduced from the fact that cooling of the α form, directly obtained by the transformation of this phase on heating, did not restore it, even after 1 d at low temperature (data not shown). Identification of the transitions that correspond to each endotherm is reported in Figure 5C. The endotherm between 16 and 19°C was related to the melting of α (form II, according to Tables 1 and 2) and thus associated with the decrease of the lines at 48.5 and 4.22 Å. The last endotherm, recorded above 25°C, corresponds to melting of the variety that exhibits a spacing at 44.9 Å, presumably some form IV (according to Tables 1 and 2). In between, overlapping of the exotherm that corresponds to the formation of this last form (also indicated by α → β′) and of the endotherm maximum of α melting results in this complex recording in which the peaks are not separated. The dashed line indicates

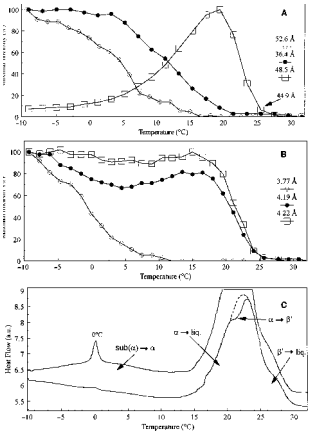


**FIG. 5.** Simultaneous XRD as a function of temperature (XRDT) and DSC recordings. Evolution of the main (A) long- and (B) short-spacings, recorded in Figure 4 during heating at 1°C/min of two samples quenched at −10°C; the corresponding DSC recordings (C) were obtained from the two different samples used for A and B recordings but with a different sensitivity of the recorder; for explanation of dotted line see text. See Figure 3 for other abbreviation.

the peak that might have been recorded in absence of the exotherm (41). The respective enthalpies of the peaks and their XRDT intensities indicate that the monotropic α(II) →β′(IV) transition was not complete, so that only part of the more stable form (β′) was formed under the experimental conditions.

*Intermediate forms. Low heating rate (0.1°C/min).* A similar experiment was carried out by quenching the CB at −30°C but heating it at 0.1°C/min between −10 and 38°C, instead of 1°C/min as above. Contrary to the previous experiments and because of the duration of the run at 0.1°C/min (about 8 h), only one XRDT recording was performed with the synchrotron beam at short sample-detector distance. The initial XRD pattern shows the same intense sharp lines at 52.4, 26.2, 4.19, and 3.74 Å and two broad peaks at 111.2 and 36.5 Å. Figures 6A and 6B report intensity variations of the main spacings as a function of temperature. At 0.1°C/min, the lines that corresponded to the spacing at 52.4 Å completely vanished in the range of 0–15°C, while the line at 48 Å reached its maximal intensity at 15°C. The broad peak, the

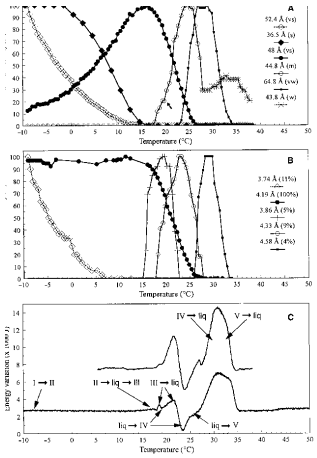


**FIG. 6.** Simultaneous XRDT and DSC recordings. Evolution of the long- and short-spacings of CB as determined by (A) small- and (B) wide-angle XRD during heating at 0.1°C/min of two samples quenched from 80 to –10°C. The arrow indicates the inflection point in the intensity increase of the line at 44.8 Å. Relative intensities of the peaks are given on the graph within parentheses (100% corresponds to the strongest peak) or noted as vs (very strong), s (strong), m (medium), w (weak), and vw (very weak). (C) Corresponding DSC recordings (upper curve, simultaneous XRDT and DSC recordings; lower curve recorded 1 d later with a Perkin-Elmer (DSC-7; St. Quentin en Yvelines, France). See Figures 3 and 5 for other abbreviations.

maximum of which was observed at 36.5 Å, seemed to decrease later than the lines at 52.4 Å and 3.74 Å (the temperature-dependent evolutions of which are again associated), while the intensity of the line at 4.19 Å stayed constant with a small shift to 4.20 Å (not shown). Starting from 18°C, the spacing at 48 Å was progressively transformed to yield that at 44.8 Å, which reached its maximum at 25°C. During this phase transition, a small line at 4.33 Å appeared between 18 and 28°C with an evolution similar to that of the spacing at 44.8 Å. At 23°C, a spacing at 64.8 Å began to increase to reach its maximum between 27 and 29°C, just after the spacing at 44.8 Å vanished, and it disappeared at 33–34°C. This spacing can be correlated to the line at 4.58 Å, which was observed between 26 and 33.5°C. The increase of the line at 43.8 Å above 28°C corresponds to crystallization of trisaturated TAG discussed above. The persistence of this line beyond 38°C at low heating rates confirms that high-melting crystals may coexist within the liquid and be in equilibrium with the latter.

According to Tables 1 and 2, the lines at 48 and 4.22 Å, 45 and 4.33 Å, 64.8 and 4.58 Å can be identified as the Forms II, IV, and V of CB, respectively. Attribution of the other lines is more difficult and will be discussed later.

The corresponding thermal analysis, either recorded simultaneously with XRDT as above or later with the DSC-7 are reported in Figure 6C. The two recordings were identical and can be interpreted with the help of the XRDT recordings as above. The large endotherm observed between 27 and 34.5°C corresponds to melting of Form V. The complex exotherm preceding this peak is mainly attributable to crystallization of this Form V starting at about 25°C. The expected enthalpy of this exotherm should have been, more or less, the same as that of the melting endotherm. This indicates that melting of Form IV and crystallization of Form V overlap, which is also indicated by XRDT (Figs. 6A and 6B). As above, only the resulting thermal event is recorded (41). The beginning and the end of these Z-shaped curves correspond to melting of the less-stable species (endothermic) and to crystallization of the more-stable one (exothermic). The intermediate part of the curve results from the sum of the two thermal events. The same analysis can be tentatively applied to the two preceding Z-shaped resulting curves. The first observable transition (between 15 and 18°C) is an endotherm that corresponds to the melting of Form II ($\alpha$), which precedes an exotherm (seen as a first decrease of the $\alpha$ endotherm around 16–18°C) and presumably corresponds to partial recrystallization of the liquid into Form III. Crystallization of Form IV starts at 18°C before the completion of crystallization of Form III at 19°C, as shown by both Figures 6B and 6C. The two exotherm transitions, corresponding to the formation of Forms III and IV, are close and overlap with melting of II and III, respectively. Some of the variations of intensity reported in Figures 6A and 6B cannot be used reliably for quantitative evaluation of the existing varieties because there is also overlapping of peaks in XRDT (for instance, decreases of the lines characterizing the $\alpha$ form, at both 4.19 and 48 Å, observed above 15°C cannot be used to follow its melting because of their closeness to other lines). Nevertheless, the inflection point, observed in the increase of the intensity peak recorded at 44.8 Å (Fig. 6A), delimits two domains of crystal growth. The first one can be associated with either the presence of a line at 3.86 Å, and thus connected to the formation of Form III, or to the formation of Form IV from the liquid phase. The domain of temperature in which the spacing at 3.86 Å was recorded corresponds exactly to the first intensity jump (the amplitude of which is less than that of the second and explains the respective enthalpies/peak surfaces observed in Fig. 6C); it vanishes at exactly the inflection point of the spacing at 44.8 Å (Figs. 6A and 6B, respectively). The absence of an inflection point during the decrease of the line at 48 Å indicates that Form III develops at the expense of Form II but with the same long-spacing. The

second part of the curve is associated with the presence of the line at 4.33 Å and corresponds to variety IV of CB (Tables 1 and 2).

Also, a small endotherm, observed between 42.5 and 47°C on the DSC-7 recordings, might be related to melting of the trisaturated TAG (43.8 ± 1 Å). At higher heating rates, such as 0.5 or 1°C/min, a broad peak, centered at about −3°C, was clearly recorded between −10 and 5°C (not shown). This hump, which was also observed around −10°C at 0.1°C/min in the DSC-7, may be interpreted as an endotherm associated with the decrease of lines at 52.4, 3.74, and 36.5 Å and their evolution to give the line at 48 Å.

*Intermediate cooling and heating rates (2°C/min).* The formation of intermediate forms also has been studied at intermediate cooling rates, close to those used in chocolate manufacturing, to get a better understanding of industrial crystallization processes. A liquid CB sample was first cooled from 40 to 0°C at 2°C/min and reheated to 40°C at the same rate. Figures 7A and 7B show the three-dimensional plots obtained by XRDT for crystallization and fusion, respectively. As previously, the intensity of each short- and long-spacing was plotted as a function of temperature (Figs. 7C and 8). Crystallization begins by the appearance of a small line at 49.6 Å, observed from about 20–22°C, which shifts slowly to about 48.5 Å as it develops. This line can be related to the exotherm that appears at about 19°C in the DSC recording (Fig. 3A), which was interpreted as the crystallization of trisaturated TAG. The spacing of 49.6–48.5 Å is close to the value given by Lavigne *et al.* (31) for the α form of StStSt (50.6 Å) and confirms that trisaturated TAG first crystallize in their α form before transforming into the β form.

Figures 7A and 7C also show that the major part of CB crystallizes at about 15°C into a highly unstable form that is characterized by the lines at 52.9 and 52.9/2 Å after partial crystallization in the α form (48.5 Å). The growth of the lines at 52.9 and 52.9/2 Å was accompanied by formation of a bump between the two sharp lines. This unstable form corresponds to the liquid-crystalline organization of the TAG discussed above (Fig. 4A). During cooling (Figs. 7A and 7C), the unstable form progressively transformed into α (49.5 Å) between 10 and 0°C. Evolution of the short-spacings recorded as a function of temperature shows that the lines at about 53 and 48.5 Å were related to those at 3.84 and 4.18 Å, respectively. During heating (Figs. 7B and 7C), these unstable forms successively vanished at about 9 and 20°C, while a spacing at 45 Å, which corresponds to the β′ form (IV) of CB or to the β form of trisaturated TAG, persisted until about 28°C. The constant value observed for the line at 3.84 Å between 10 and 22°C is due to closeness of the neighboring peak at 4.18 Å.

Another experiment was carried out under the same conditions with a CB sample that contained 2% of StStSt to observe the influence of trisaturated TAG on its crystallization (Fig. 8). The trisaturated TAG started to crystallize in their α form at a higher temperature than in the absence of StStSt between 30 and 25°C, but crystallization of monounsaturated TAG of CB in Forms I (sub-α, 53 Å) and II (α, 48.5 Å) was

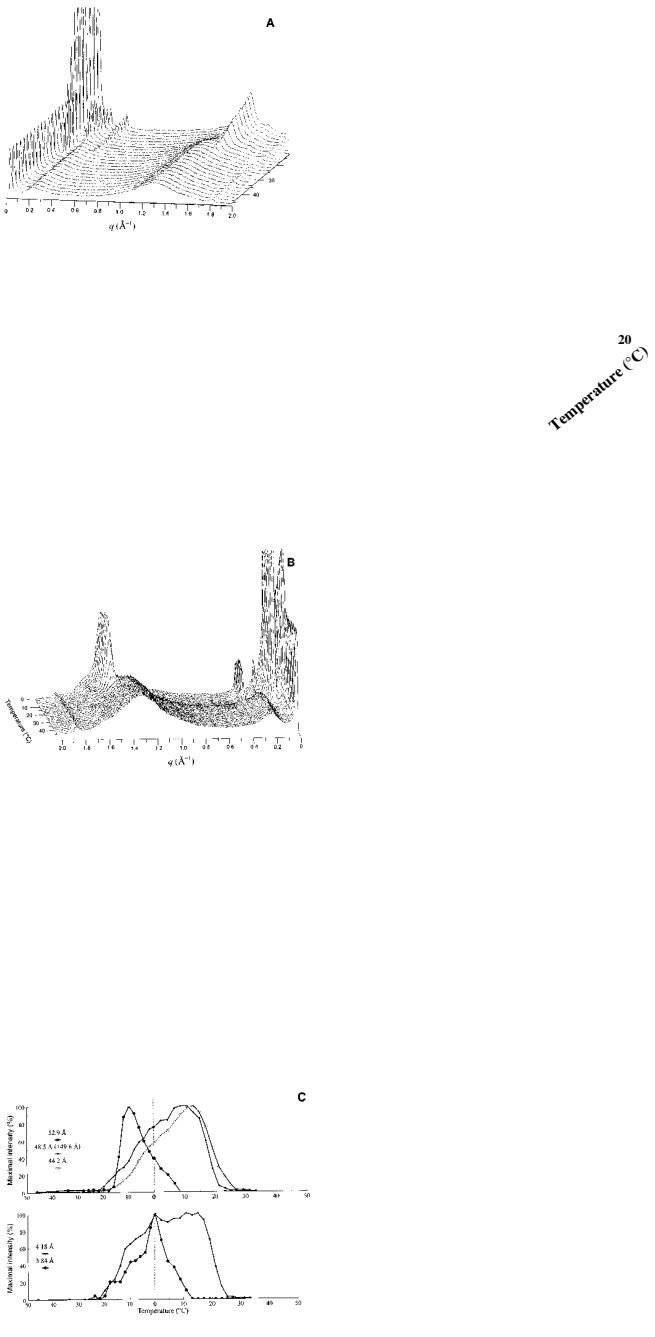


**FIG. 7.** Wide-angle XRD as a function of temperature. The three-dimensional plots were obtained from the XRD patterns recorded during crystallization and subsequent fusion of CB at cooling (A) and heating (B) rates of 2.0°C/min. (C) Evolution of the long- and short-spacings during crystallization (left) and subsequent fusion (right) of CB during experiments (A) and (B). (Intensities of the lines at 49.6 and 48.5 Å are plotted together). See Figure 1 for abbreviations.

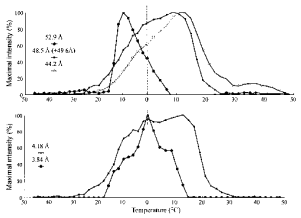

**FIG. 8.** Evolution of the long- and short-spacings during crystallization (left) and subsequent fusion (right) of CB with 2% tristearin (StStSt) as determined by wide-angle XRD as a function of temperature during cooling and heating at 2.0°C/min. (Intensities of the lines at 49.6 and 48.5 Å are plotted together.) See Figure 1 for abbreviations.

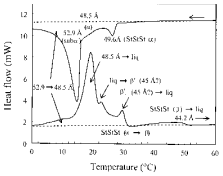

**FIG. 9.** DSC recordings on cooling and heating at 2°C/min to show different crystallization and fusion observed with a CB sample that contained 2% StStSt. See Figures 1, 3, and 8 for abbreviations.

not accelerated. Furthermore, during heating at 2°C/min, the melting temperatures of these unstable forms were not shifted by more than 1°C. The main consequence of StStSt addition was evolution of the line at 44 Å, which increased above 30°C, with a maximum at 33°C, and only vanished at 48°C. This intensity increase results from the polymorphic transition of the trisaturated TAG from α to β form as observed previously (Fig. 3B, HMF). The slow kinetics of the transition, as well as the temperature at which it was observed, suggests that it is favored when the monounsaturated TAG are completely melted, or in others words, when the liquid content is high enough to partly solubilize the trisaturated TAG. Figure 9 shows the DSC curves of a CB that was enriched with 2% of StStSt as recorded during cooling followed by heating at the same rates as above (2°C/min) (Fig. 8). With the help of XRDT recordings, all thermal phenomena were identified (as reported in Fig. 9), although two of them are still tentative. The endotherm between 28.5 and 30°C was related to melting of the $\beta'_1$ variety of CB (Form IV, Table 1), although the line at about $q = 0.14$ Å$^{-1}$ (45 Å) was not clearly observed (it was probably hidden by the large peak at 48.5 Å and/or fused with the line at 44.2 Å). The small endotherm, observed between 21 and 22°C on heating, probably results from the overlapping of two thermal events, corresponding to melting of the α form (48.5 Å) and recrystallization of liquid into the $\beta'_1$ form (about 45 Å, form IV, Table 1).

## DISCUSSION

Thermal XRD and DSC analysis indicated that phase separations systematically occur during CB crystallization. The main TAG segregation involves a trisaturated fraction, which partially phase-separates from the mono- and polyunsaturated species by crystallizing, as shown by chemical analysis of the fractions. However, the phase separation of polyunsaturated TAG, which remain liquid at low temperature and only crystallize at about 4°C on cooling, should also be considered because it might play an important role in the evolution of unstable CB polymorphs, as well as in chocolate blooming (40). Although the main TAG segregation in the solid state has only been observed when CB crystallizes into the Forms II and V (the form in which chocolate is usually commercialized), it probably also occurs with some other forms, such as VI (19,21,22). This behavior may be explained by the low solubility of the trisaturated TAG within the monounsaturated TAG, which represent more than 80% of CB (42). These results agree with the "memory effect" of CB as reported by van Malssen (24). This author observed that, depending on its origin, CB needed to be heated beyond a minimal temperature between 34 and 38°C to restore its original properties. Below this temperature, high-melting crystals may persist in liquid CB and modify its crystallization behavior during storage at 25°C. However, the above observations show that these high-melting crystals are mainly composed of trisaturated TAG and not StOSt (24). Thus, the lower and higher memory melting points reported by this author correspond to trisaturated TAG contents of 1.0 and 2.8%, respectively, which correlates perfectly with our results.

The separate crystallization of trisaturated TAG also agrees with observations of Dimick and Manning (43) and later of Davis and Dimick (25,26) who reported that CB crystallization starts from that of HMF which are composed mainly of complex lipids and these TAG. However, the phase separations that they observed were obtained during a static crystallization at 26.5°C of several hours. Under these conditions, the high-melting crystals, observed at 72.4°C, apparently correspond to the crystallization of the β form of trisaturated TAG. Our results show that, during the tempering process of chocolate when CB crystallizes within a few minutes, the crystallization of the trisaturated TAG probably oc-

curs *via* the α form. This crystallization was only revealed at the long-spacing level; no short-spacing (expected at about 4.20 Å) was observed. This was also true above 35°C for melting of the β form of trisaturated TAG, for which a strong short-spacing was expected at 4.58 Å. This might be due to a lack of sensitivity at wide angles, while the concentration of crystals to detect is very small despite the high flux of the X-ray source, rather than to the fact that long-spacings are organized first during crystallization (K. Sato, personal communication).

The observation by XRDT, and also by DSC, of the formation of the different forms during heating, as previously reported by Wille and Lutton (10), including Form III, the existence of which has been discussed several times (7,10,19,21,22), unambiguously confirms the pertinence of their description of CB polymorphism.

Fast cooling (about 100°C/s) of melted CB results in the formation of a phase that is less organized than the α form, but it transforms irreversibly into the latter on heating. At −10°C, its diffraction/scattering pattern (Fig. 4) decomposes into a set of two strong and sharp diffraction lines ($\Delta_{1/2}$ = half-height widths of lines, expressed in $Å^{-1}$) at $q$ = 0.12 $Å^{-1}$ (52.6 Å, $\Delta_{1/2}$ = 0.004 $Å^{-1}$) and 0.24 $Å^{-1}$ (26.3 Å, $\Delta_{1/2}$ = 0.006 $Å^{-1}$), and a series of broad peaks at $q$ = 0.06 $Å^{-1}$ (112 Å, $\Delta_{1/2}$ = 0.040 $Å^{-1}$) and 0.17 $Å^{-1}$ (36.4 Å, $\Delta_{1/2}$ = 0.057 $Å^{-1}$). The short-spacings, which indicate a packing more compact than the hexagonal arrangement of the α form, correspond to a β′ type (4.19 Å, $q$ = 1.5 $Å^{-1}$ and 3.77 Å, $q$ = 1.67 $Å^{-1}$, $\Delta_{1/2}$ = 0.05 $Å^{-1}$). Such a pattern, showing the coexistence of sharp and broad lines, cannot be explained by a single organization of the chains. Therefore, assuming that the two sharp peaks correspond to the $d_{001}$ and $d_{002}$ diffraction lines of a lamellar structure (with a 52.6 Å spacing), the values of half-height widths found for these peaks, both for long- and short-spacings ($\Delta_{1/2}$ = 0.005 ± 0.001 and 0.05 $Å^{-1}$, respectively), are less than that found for α (48.5 Å, $\Delta_{1/2}$ = 0.016 $Å^{-1}$ and 4.22 Å, $\Delta_{1/2}$ = 0.06 $Å^{-1}$). This indicates that the packing of this moiety of the sub-α organization is more compact than that of α. The broad peaks, the main one of which is centered at about 36.5 Å, probably result from scattering by poorly oriented chains. This organization, which displays maxima at $q$ = 0.06 $Å^{-1}$ (112 Å) and $q$ = 0.17 $Å^{-1}$ (36.4 Å), is less organized than the α form but more than the liquid, as shown by both lines' positions, for instance at smaller angles than the hexagonal short-spacing of α, and larger half-height widths ($\Delta_{1/2}$ = 0.09 for the broad peaks of the liquid phase of CB and $\Delta_{1/2}$ = 0.057 $Å^{-1}$ for the less-organized moiety of the liquid crystalline phase).

Some of the lines of this pattern have been observed previously. They were assigned to the sub-α (Table 1) and/or β′ (sub-α) (7) form of CB by these investigators, to focus either on the relative metastability of this form compared to α and/or on its typical short-spacing pattern. In fact, such a complex pattern may be attributed either to the coexistence of two different structures, each of them displaying part of the scattering/diffraction peaks discussed above, or to a single liquid crystalline organization that combines both types of characteristics.

The coexistence of two distinct structures would have shown two different patterns of thermal behavior, which were not observed. Moreover, no sharp transition was observed when this variety transformed into α. On the contrary, according to XRDT and DSC recordings (Figs. 4 and 5), the transition was gradual and, whatever the heating or cooling rate used, it always occurred between −10 and 15°C. Although the sample-detector distance used (almost 1.5 m) allowed excellent line separation, it was not enough to achieve full separation of the 48.5 and 52.5 Å lines and to determine the transition temperature more precisely by XRDT. In fact, in contrast to the usual solid-liquid-solid transition, which is observed for monotropic substances at the melting point of an unstable form (31), the metastable form is here progressively replaced by α. Moreover, some intermediate recordings show the two X-ray patterns superimposed (in the range of 5–10°C, Fig. 4), making line separation difficult without a specific mathematical model. This gradual transition agrees with the observations made by Riiner (7) that it is time- and temperature-dependent.

This thermal behavior favors the hypothesis of the existence of a single form rather than that of a mixture of two. However, how can the coexistence of the two organizations discussed above in the same phase be explained? The fact that the whole organization is less stable than α and nevertheless that part of it corresponds to a phase much more ordered than α indicates, as a counterpart, that only a part of the structure is ordered, while the rest is not. This is coherent with the existence in the X-ray pattern of several broad lines that correspond to scattering from the unorganized component of the structure. The disordered moiety exhibits broad peaks that resemble those scattered by micellar structures with aliphatic chains in the liquid state (44). The observation of a broad bump at the bottom of the short-spacing lines, probably due to some smectic liquid-crystalline organization of part of the chains, confirmed this interpretation (Fig. 4A). The organization of the ordered moiety is probably lamellar, as indicated by the presence of sharp first- and second-orders for the long-spacings, with an O⊥ subcell. Thus, this coorganization might correspond to a partly crystallized, partly liquid crystalline structure, the chains in the latter being organized by their covalent links with the crystalline lattice (as in a brush). In such an organization, the mobility of the liquid chains is only allowed at methyl-end group extremity.

These peaks also can be compared to those found for the TAG in the liquid state, which are located at mean $q$ = 0.27 $Å^{-1}$ (23.75 ± 0.10 Å) $\Delta_{1/2}$ = 0.09 $Å^{-1}$ and $q$ = 1.36 $Å^{-1}$ (4.57 ± 0.01 $Å^{-1}$) $\Delta_{1/2}$ = 0.31 $Å^{-1}$ at 30°C for CB. These last peaks are broader and weaker in intensity than those found for the less-ordered part of this phase, as expected according to the above hypothesis, for liquid chains that are connected to a strongly organized (crystalline in this case) lattice. The main difference between the two liquids originates in the planar nature of the lattice limit compared to the probably fluc-

tuating surface made by the glycerol groups of the TAG in the liquid state (3,8). Such an organization also can be compared to that shown by phospholipids, such as phosphatidylcholine, in the liquid crystalline state (Lα). Above the temperature of their main transition, the phospholipid chains are liquid and maintained partly organized by the electrostatic links of the polar head groups (45). However, the X-ray pattern shown by egg phosphatidylcholine in Lα in excess water, although similar at the short-spacing level, is much more ordered in the chain direction, as shown by its peak width.

Although calculation made from model organization is needed to solve the structure of this phase, a scheme of a hypothetical arrangement of the TAG molecules is given in Figure 10. The possibility of an arrangement of the TAG within aggregates has not been addressed because the sharp decrease of the intensity observed at low $q$ (Fig. 4A) indicates that they are rather large, if they exist. Also, this scheme does not explain the exact origin of the sharp lines observed at a spacing of about 52.6 Å, which are incompatible with the usual model of TAG crystallization, this period being too long for a 2L organization and too short for 3L. It associates two levels of organization, a crystalline and a liquid-like moiety. Such a structure may explain why, on rapid cooling starting from the liquid fat, only part of the chains has time to crystallize while the other part does not. Moreover, the degree of freedom in the molecular mobilities left by the liquid part of the organization allows the other moiety to crystallize rapidly into a compact subcell. For comparison, formation of the β′ form of StStSt takes a minimum of about 10 min and has complex time–temperature conditioning requirements; the situation is similar for the TAG-like 1,3-palmitoyl-2-stearoylglycerol (PStP), which displays only the β′ form (and α). Moreover, the behavior of this last TAG, compared with, for instance, its homolog 1-stearoyl-2,3-palmitoylglycerol (StPP), which preferentially exhibits the β form, is a good illustration of the close relationship between the positioning on the glycerol of fatty acids of different chainlengths and the orientation of their crystallization toward a particular subcell (4,46). Indeed, the fast formation of the β′ organization is in favor of some liquid surrounding the molecule extremities.

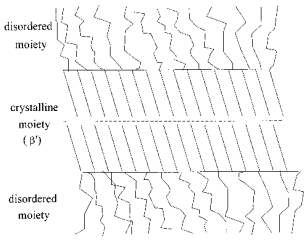


**FIG. 10.** Scheme of a possible arrangement of the triacylglycerol (TAG) molecules in the sub-α form. A crystalline moiety with a planar organization involves the glycerol backbone and saturated fatty acid chains, while the remaining acyl groups (mono- and polyunsaturated) adopt a liquid-like structure.

On the other hand, the presence of a liquid crystalline moiety in the structure also would explain its progressive transition into the α form because it is well known that the presence of a liquid favors the evolution of unstable species toward more stable forms (47). On cooling at 2°C/min, the α form starts to crystallize before the liquid-crystalline phase (Figs. 7A, 7C, 9). Therefore, the latter probably corresponds to aggregation of the molecules not frozen in α form. The sub-α → α transition, which is favored at slow cooling rates by the presence of some α in mixture with sub-α, occurs more or less rapidly in the range of −10 to 15°C and thus raises the question of chain mobility and organization at lower temperatures in relation with the stability of this phase.

The second consequence of the existence of such a compact and well-structured (sharp long-spacings) organization is that presumably the liquid from which it forms could be already preorganized. So, taking into account the respective temperatures of crystallization of chains, the saturated ones would crystallize first, leaving the unsaturated chains in the liquid state. This preorganization assumes that: (i) the liquid state of CB, as other liquid fats, is liquid crystalline and rather of the smectic type (3,48) than nematic (9), (ii) its organization corresponds to layers (or flat aggregates) made from saturated chains, while other parts contain the unsaturated chains. The liquidus shapes observed in some binary phase diagrams of TAG, almost horizontal on the side of the thermally more stable component with a marked change of slope when approaching the concentrations rich in the second component, already have been proposed as reflecting some kind of phase separation in the liquid medium (36). Such a liquidus shape is frequently observed for saturated-unsaturated TAG (or saturated-partly unsaturated) binary phase diagrams on the saturated side (for instance with StStSt-triolein or StStSt-StOSt) (42).

*Comparison with palm oil.* The existence of a liquid crystalline phase, obtained by very fast cooling, was not found in pure TAG, such as triolein, StStSt and even POP, which is nevertheless one of the major constituent of CB, because they all readily crystallize in the α phase (1,13). However, we found that palm oil and lard, which are, like CB, mainly composed of a mixture of monounsaturated and saturated TAG, also show partial crystallization. The propensity of fats to crystallize in sub-α(β′) carefully has been investigated by Riiner (7) by means of temperature-programmed XRD camera recordings. Among 30 oils and fats of food technological interest, he found that five display this property, namely, beef tallow, CB, lard, palm oil, and sheanut butter. Except this last, all these fats have intermediate iodine values; fats and oils with lower and higher iodine values do not display such behavior.


**FIG. 11.** Small-angle X-ray patterns obtained for pure fats and their olein and stearin fractions, CB (A) and palm oil (B). See Figure 1 for abbreviations.

The small-angle XRD patterns of palm oil and its fractions (olein and stearin) were recorded, at –30°C after quenching as above, for comparison with that of CB obtained by fractionation (see above) (Fig. 11A,B). Weak differences were observed between HMF, LMF, and CB itself. HMF showed a broad peak at about 36 Å ($q = 0.18$ Å$^{-1}$), reduced in intensity, but an increase of the spacings at 52.1 Å ($q = 0.12$ Å$^{-1}$), associated with important broadening compared to the other fats. Palm oil and its fractions exhibited similar behavior, except that, for the stearin fraction, the liquid-crystalline phase (55, 55/2 Å, and broad peak at 36 Å) was mixed with the α form (48.5 Å). This pattern also revealed a weak but sharp peak at 111 Å (Fig. 11B), which seems to be related to the sharp peaks at spacing 55 Å rather than to the α form. For all samples, whatever the fat and the fractions considered, the intensities of the sharp and scattering peaks are approximately in the same proportions. However, pure CB exhibits the highest intensity for the scattering peak, even compared to its fractions.

The relationship between the formation of this liquid crystalline phase and the fat composition is still unclear. Obtaining this phase seems related to: (i) the presence of a mixture of TAG and (ii) a specific unsaturated/saturated fatty acid ratio.

*Thermodynamic considerations.* Further evidence for an organization of the liquid that was not mentioned before is provided by calculations from thermodynamic data. First, the plot of melting enthalpies of TAG of the same family, such as trisaturateds with a single fatty acid (trilaurin to tribehenin), as a function of carbon number revealed that a constant number of methylene groups (about two per aliphatic chain) and the glyceryl carbons do not participate in the melting enthalpy. (The negative term found in the linear relationship between melting enthalpy of the β form of trisaturated TAG cannot be attributed to some disorganization of this solid phase because it has been shown by XRD that all these TAG display the same basic structure, derived from that of LLL.) Then, taking into account the importance of this nonmelting fraction, it must be related to some liquid organization (41,49).

Second, evidence arises from the plots of the molar volume of the trisaturated TAG in the solid (β form) and liquid states (at 80°C) as a function of their molecular weights. These molar volumes were deduced from their liquid and solid densities taken from the literature (45, from Table 10-3). Both series of molar volumes vary linearly with the molecular weights of the corresponding TAG.

The two equations deduced from the linear regression are shown with their corresponding plots in Figure 12. The negative value (–53.4 cm$^3$) observed for the plot of the liquid state already shows that a rather high density is expected for the polar headgroup packing, while the positive value found for the β form tends to indicate the reverse for this solid phase (neglecting, for this comparison, the dilation of β solid phase between the temperatures at which molar volumes were measured and 80°C). Taking into account the fact that, except for

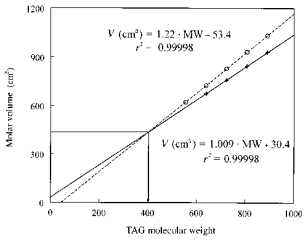


**FIG. 12.** Plots of the molar volumes of TAG in the liquid (solid line) and solid (dashed line) states deduced from literature data. See Figure 10 for abbreviations.

the liquid phase, the data are not taken at the same temperature (but thermal expansion is rather low in the solid phase), the intercept of the two straight lines is found at a high molecular weight (about 400). That the volumes below this intercept are occupied by polar groups in both states and are equivalent (about 400 $cm^3$/mole) indicates that the first carbons of the chains are not disorganized by chain melting. This confirms that the polar groups and parts of the chains of trisaturated TAG in the liquid state are as dense as the equivalent moiety of the crystalline form in its most compact packing. These two independent lines of evidence for liquid organization favor the hypothesis of a smectic organization of the liquid, as reported by Larsson (8), in particular because the high density found for the polar head- groups is unlikely to correspond to their dilution in a paraffinic environment.

In conclusion, fast cooling of fats, mainly composed of monounsaturated TAG, such as CB and palm oil, leads first to the formation of a liquid crystalline phase, which is probably partly organized as a crystal with a compact subcell of β′ type and partly as a liquid. This organization, which likely also forms from other monounsaturated-rich TAG fats, is also obtained for CB at moderate cooling rates below 15°C. In spite of the presence of a more organized moiety, the existence of a liquid-crystalline part in the structure makes it on the whole less stable than α, into which it progressively transforms when maintained in the range of 0–15°C.

The partial fractionation of the StStSt TAG of CB observed in this study develops independent of the presence of this phase and others. The persistence of crystals, mainly composed of trisaturated TAG when the other moiety of CB is liquid, explains the specific thermal behavior previously observed (25,26). This phase separation in the solid state does not affect the validity of the nomenclature proposed by Wille and Lutton (10), especially because the six forms that they described have been reidentified. However, it should serve as a reminder that even for CB, which is a specific fat mainly composed of three similar monounsaturated TAG, it only describes the behavior of its main fraction and not the whole fat. Therefore, for natural fats of generally more complex composition and polymorphism that display simultaneous complex arrangements made from different classes of TAG in addition to a liquid fraction, as recently shown for anhydrous milk fat and its fractions (35), a single denomination should be avoided.

On the other hand, these results show that, even for fats that display a simple composition, the interpretation of thermal analysis is difficult, especially when numerous polymorphic transitions occur successively. In this respect, the use of X-ray (or neutron) diffraction/scattering techniques, preferably recorded as a function of temperature, by allowing continuous identification of the crystal structures formed, is absolutely necessary for understanding these phenomena.

## ACKNOWLEDGMENTS

C. Loisel was supported by a grant from Association Nationale de la Recherche Technique (A.N.R.T., Convention Cifre) and Groupe Danone for Ph.D. preparation (50). We thank G. Barratt for her critical reading of the manuscript.

## REFERENCES

1. Sato, K., T. Arishima, Z.H. Wang, K. Ojima, N. Sagi, and H. Mori, Polymorphism of POP and SOS. I. Occurrence and Polymorphic Transformation. *J. Am. Oil Chem. Soc. 66*:664–674 (1989).
2. Chapman, D., *The Structure of Lipids by Spectroscopic and X-ray Techniques*, Methuen, London, 1965, pp. 221–315.
3. Larsson, K., Molecular Arrangement in Glycerides, *Fette Seifen Anstrichm. 74*:136–142 (1972).
4. Lutton, E.S., Lipid Structures, *J. Am. Oil Chem. Soc. 49*:1–9. (1972).
5. Garti, N., and K. Sato, *Crystallization and Polymorphism of Fats and Fatty Acids—Surfactant Science Series*, Vol. 31, Marcel Dekker Inc., New York, 1988.
6. Ollivon, M., Triglycérides, in *Manuel des Corps Gras*, Lavoisier, Paris, 1992, pp. 469–503.
7. Riiner, U., Investigation of the Polymorphism of Fats and Oils by Temperature Programmed X-Ray Diffraction, *Lebensm. Wiss. Technol. 3*:101–106 (1970).
8. Larsson, K., On the Structure of the Liquid State of Triglycerides, *J. Am. Oil Chem. Soc. 69*:835–836 (1992).
9. Cebula, D.J., D.J. McClements, M.J.W. Powey, and P. Smith, Neutron Diffraction Studies of Liquid and Crystalline Trilaurin, *Ibid. 69*:130–136 (1992).
10. Wille, R.L., and E.S. Lutton, Polymorphism of CB, *Ibid. 43*: 491–496 (1966).
11. Kunutsor, S.K., and M. Ollivon, Ternary Phase Diagram of β Stable Forms of Major Triglycerides of CB (POP, POS, SOS), 16th ISF Research World Congress, edited by J. Hollo, Budapest, 1983, p. 11.
12. Sato, K., Physical and Molecular Properties of Lipid Polymorphs—A Review, *Food Microstructure 6*:151–159 (1987).
13. Arishima, T., N. Sagi, H. Mori, and K. Sato, Polymorphism of POS. I. Occurrence and Polymorphic Transformation, *J. Am. Oil Chem. Soc. 68*:710–715 (1991).
14. Duck, W., The Measurement of Unstable Fat in Finished Chocolate, *Manufacturing Confectioner 35* (6):67–72. (1964).
15. Chapman, G.M., E.E. Akehurst, and W.B. Wright, Cocoa Butter and Confectionery Fats. Studies Using Programmed Temperature X-Ray Diffraction and Differential Scanning Calorimetry, *J. Am. Oil Chem. Soc. 48*:824–830 (1971).
16. Adenier, H., M. Ollivon, R. Perron, and H. Chaveron, Le blanchiment gras. I. Observations et commentaires, *Chocolaterie Confiserie de France 315*:7–14 (1975).
17. Huyghebaert, A., and H. Hendrickx, Polymorphism of Cocoa Butter, Shown by Differential Scanning Calorimetry, *Lebensm. Wiss. Technol. 4*:59–63 (1971).
18. Lovegren, N.V., M.S. Gline, and R.O. Feuge, Polymorphic Changes in Mixtures of Confectionery Fats, *J. Am. Oil Chem. Soc. 53*:83–88 (1976).
19. Merken, G.V., and S.V. Vaeck, Etude du polymorphisme du beurre de cacao par calorimétrie DSC, *Lebensm. Wiss. Technol. 13*:314–317 (1980).
20. Davis, T.R., and P.S. Dimick, Solidification of Cocoa Butter, *Proc. PMCA Prod. Conf. 40*:104–108 (1986).
21. Schlichter-Aronhime, J., and N. Garti, in *Crystallization and Polymorphism of Fats and Fatty Acids*, Surfactant Science Series, Vol. 31, edited by N. Garti and K. Sato, Marcel Dekker Inc., New York, 1988, pp. 363–393.
22. Schlichter-Aronhime, J., S. Sarig, and N. Garti, Reconsideration of Polymorphic Transformations in Cocoa Butter Using DSC, *J. Am. Oil Chem. Soc. 65*:1140–1143 (1988).

23. Becker, K., Les causes du blanchiment gras par les matières grasses du chocolat et des bonbons au chocolat, *Rev. Int. Choc. 1*:250–254 (1957).
24. van Malssen, K.F., Real-Time X-Ray Powder Diffraction Applied to Cocoa Butter and Graphite Intercalates, Ph.D., Amsterdam University, 1994.
25. Davis, T.R., and P.S. Dimick, Crystals Formed During Cocoa Butter Solidification, *J. Am. Oil Chem. Soc. 66*:1488–1493 (1989).
26. Davis, T.R., and P.S. Dimick, Lipid Composition of High-Melting Seed Crystals Formed During Cocoa Butter Solidification, *Ibid. 66*:1494–1498 (1989).
27. Chaiseri, S., and P.S. Dimick, Dynamic Crystallization of Cocoa Butter. I. Characterization of Simple Lipids in Rapid- and Slow-Nucleation Cocoa Butters and Their Seed Crystals, *Ibid. 72*: 1491–1496 (1995).
28. Chaiseri, S., and P.S. Dimick, Dynamic Crystallization of Cocoa Butter. II. Morphological, Thermal and Chemical Characteristics During Crystal Growth, *Ibid. 72*:1497–1504 (1995).
29. Cebula, D.J., K.M. Dilley, and K. Smith, Continuous Tempering Studies on Model Confectionery Systems, *PMCA Production Conference 45*: 42–47 (1991).
30. Kellens, M., W. Meeussen, C. Riekel, and H. Reynaers, Time-Resolved X-ray Diffraction Studies of the Polymorphic Behaviour of Tripalmitin Using Synchrotron Radiation, *Chem. Phys. Lipids. 52*:79–98 (1990).
31. Lavigne, F., C. Bourgaux, and M. Ollivon, Phase Transition of Saturated Triglycerides, *J. Phys. IV*, Colloque C8, *sup. au J. Phys. I. 3*:137–140 (1993).
32. van Gelder, R.N.M.N., N. Hogdson, K.J. Roberts, A. Rossi, M. Wells, M. Polgreen, and I. Smith, Crystallisation and Polymorphism in Cocoa Butter Fat: *In-situ* Studies Using Synchrotron Radiation X-ray Diffraction, in *Crystal Growth of Organic Materials,* ACS Conference Proceedings Series, edited by A.S. Myerson, 1996, pp. 209–215.
33. Sato, K., in *Advances in Applied Lipid Research*, Vol. 2, edited by F. Padley, JAI Press Inc., 1996, pp. 213–268.
34. Keller, G., F. Lavigne, C. Loisel, M. Ollivon, and C. Bourgaux, Investigation of the Complex Thermal Behavior of Fats. Combined DSC and X-ray Diffraction Techniques, *J. Thermal Anal. 47*:1–21 (1996).
35. Lavigne, F., Polymorphisme et transitions de phases des Triglycérides. Applications aux propriétés thermiques et structurales de la matière grasse laitière anhydre et de ses fractions, Ph.D. Université Paris VII, Paris XI et E.N.S.I.A, 1995.
36. Ollivon, M., and R. Perron, Etude de mélanges binaires de triglycérides dérivés des acides palmitique et stéarique, *Chem. Phys. Lipids, 25*:395–414 (1979).
37. Fraisse, B., Automatisation, traitement du signal et recueil de données en diffraction X et analyse thermique. Exploitation, analyse et représentation de données., Ph.D., Université de Montpellier II, 1995.
38. Grabielle-Madelmont, C., and R. Perron, Calorimetric Studies on Phospholipid–Water Systems. I. DL-Dipalmitoylphosphatidylcholine (DPPC) Water System, *J. Colloid Interface Sci. 95*:471–482 (1983).
39. Loisel, C., G. Lecq, G. Keller, and M. Ollivon, Dynamic Crystallization of Dark Chocolate: Influence of Temperature and Lipid Additives, *J. Food Sci.,* in press.
40. Adenier, H., H. Chaveron, and M. Ollivon, Mechanism of Fat Bloom Development on Chocolate, in *Shelf Life Studies of Foods and Beverages*; *Chemical, Biological, Physical and Nutritional Aspects*, edited by G. Charalambous, Elsevier Science Publishers B.V., 1993, pp. 353–389.
41. Ollivon, M., and R. Perron, Enthalpies and Entropies Measurements of Unstable Forms of Saturated Even Monoacid Triglycerides, *Thermochim. Acta 53*:183–194 (1982).
42. Rossell, J.B., Phase Diagrams of Triglyceride Systems, *Adv. Lipids Res. 5*:353–408 (1967).
43. Dimick, P.S., and M.D. Manning, Thermal and Compositional Properties of Cocoa Butter During Static Crystallization, *J. Am. Oil Chem. Soc. 64*:1663–1669 (1987).
44. Hayter, J.B., Physics of Amphiphiles: Micelles, Vesicles and Microemulsions, Proceedings of the International School of Physics, edited by Corti and De Giorgio, Elsevier, Amsterdam, 1985, p. 59.
45. Small, D., Glycerides, The Physical Chemistry of Lipids, in *Handbook of Lipid Research IV*, Plenum Press, New York, 1986.
46. De Jong, S., and T.C. Van Soest, Crystal Structures and Melting Points of Saturated Triglycerides in the β-2 Phase, *Acta Crystallogr.*:1570–1583 (1978).
47. Timms, R.E., Phase Behavior of Fats and Their Mixtures, *Prog. Lipid Res. 23*:1–38 (1984).
48. van den Tempel, M., Crystallization in Dispersed Systems, Physico-Chimie des composés amphiphiles, *Colloques nationaux du C.N.R.S.* n° 938, edited by R. Perron and P. Bothorel, 1979, pp. 261–264.
49. Ollivon, M., and R. Perron, *Fat Science*, 107–116 (1985).
50. Loisel, C., Physico-chimie du chocolat: cristallisation du beurre de cacao et proprietés structurales, Ph.D. Université Paris VII, Paris XI et E.N.S.I.A., 1996.

[Received October 22, 1996; accepted September 19, 1997]